# Thermal transport in a semiconductor heterostructure measured by time-resolved x-ray diffraction

Y. M. Sheu,[1] S. H. Lee,[2] J. K. Wahlstrand,[1] D. A. Walko,[3] E. C. Landahl,[3,*] D. A. Arms,[3] M. Reason,[4] R. S. Goldman,[4] and D. A. Reis[1]

[1]*FOCUS Center and Department of Physics, University of Michigan, Ann Arbor, Michigan 48109-1040, USA*

[2]*Length/Time Metrology Group, Korea Research Institute of Standards and Science, Daejeon 305-600, Republic of Korea*

[3]*Argonne National Laboratory, Argonne, Illinois 60439, USA*

[4]*Department of Materials Science and Engineering, University of Michigan, Ann Arbor, Michigan 48109-2136, USA*

(Received 17 December 2007; revised manuscript received 17 April 2008; published 21 July 2008)

We report studies of thermal transport across the interface of a semiconductor heterostructure using x-ray diffraction to measure the time-dependent lattice expansion after ultrafast laser excitation. Femtosecond laser pulses are used to rapidly and locally heat the substrate at the buried interface of an $Al_{0.3}Ga_{0.7}As/GaAs$ heterostructure grown by molecular-beam epitaxy. High-resolution time-resolved x-ray diffraction is used to study the heating and cooling of the film and substrate independently. The data are compared with a simple model for the thermal transport incorporated into dynamical diffraction calculations allowing us to extract the room-temperature cross-plane film thermal conductivity. The value is 40% lower than that extrapolated from prior results on liquid-phase epitaxy grown samples of varying concentrations.

DOI: 10.1103/PhysRevB.78.045317 PACS number(s): 68.60.Dv, 61.05.cp, 78.47.−p

There is broad interest in thermal transport in thin films and other nanoscale materials from both a fundamental physics perspective and for practical applications. In these materials, the thermal transport is often reduced compared to bulk materials potentially due to strain[1] and defects[2] as well as interfacial[3] and finite-size effects.[4] In the case of semiconductor superlattices, reduced phonon group velocity due to acoustic miniband formation[5,6] can also make contributions to the reduced thermal conductivity of the structure. However a detailed understanding of thermal transport in nanoscale materials is still a challenge both theoretically and experimentally.[7]

There is thus a great need for accurate methods to measure the thermal properties of thin films, particularly methods that can separate the various phonon transport mechanisms. A number of advanced optical techniques have been developed that use pulsed lasers as noncontact probes of high-frequency acoustic phonon propagation and heat transport.[8,9] In the time-domain thermal reflectance technique, researchers use a short laser pulse to locally heat a material, followed by a time-delayed pulse to probe changes in the temperature-dependent optical properties of the material. This has been applied to the study of thermal conductivity of thin films[10] and thermal boundary conductance of epitaxial interfaces.[11] Capinski *et al.*[6] measured cross-plane thermal conductivity in AlAs/GaAs superlattices using an optical pump-probe technique and observed a general decrease in the thermal conductivity with decreasing layer thickness, and a value that is reduced from the average alloy. Early measurements on in-plane thermal conductivity of AlAs/GaAs superlattices were performed by Yao[12] using ac calorimetric method, again showing a general decrease in thermal conductivity with decreasing layer thickness; however, they find that the in-plane thermal conductivity is better than that of the average alloy. Recently, we have utilized time-resolved x-ray diffraction (TRXD) (Refs. 13 and 14) to study the propagation of laser-generated coherent phonons across a single $Al_{0.3}Ga_{0.7}As/GaAs$ heterostructure interface.[15] In those experiments, we measured the atomic displacements associated with the strain pulse directly both for the bulk and film and found that the effect of the interface could be treated within the acoustic mismatch limit. Here, we extend these studies and report on thermal transport across this same interface. Because of the high quality of the interface, the film is fully strained and misfit dislocations are expected to be negligible. Thus, the thermal transport is expected to be dominated by the intrinsic thermal conductivity of the material. High-resolution TRXD is used to measure the time evolution of the lattice expansion as independent noncontact thermometers of the film and near-surface region of the substrate. A comparison of the data with simulations of the thermal transport enables us to extract the room-temperature cross-plane film thermal conductivity.

The experiment was conducted near room temperature on the 7ID insertion device beamline at the Advanced Photon Source (APS) synchrotron. A detailed description of the beamline, in the context of ultrafast experiments, can be found elsewhere.[15–17] Amplified Ti:sapphire laser pulses with wavelength centered at 800 nm and ~50 fs pulse duration are focused to a $\sim 2 \times 7$ mm$^2$ (full width at half maximum) spot on the sample at a 5 kHz repetition rate with up to 2 W average power. The laser is phase locked electronically to electron bunches in the storage ring such that we are able to control arbitrarily the pump-probe delay, $t$, between individual x-ray and laser pulses striking the sample with 20 ps precision.[17] The x-ray pulse train from the undulator is monochromatized with a 10 keV photon energy and a ~1.4 eV bandwidth and collimated by slits to $\sim 0.5 \times 0.5$ mm$^2$ just before the sample. Because the repetition rate of the x rays (~6.5 MHz, in 24 bunch mode) is significantly greater than that of the laser, a time-resolved detector is required. The x rays are attenuated to a level that an avalanche photodiode in photon counting mode can be used for the detector (with dead time correction). The signal from the

 

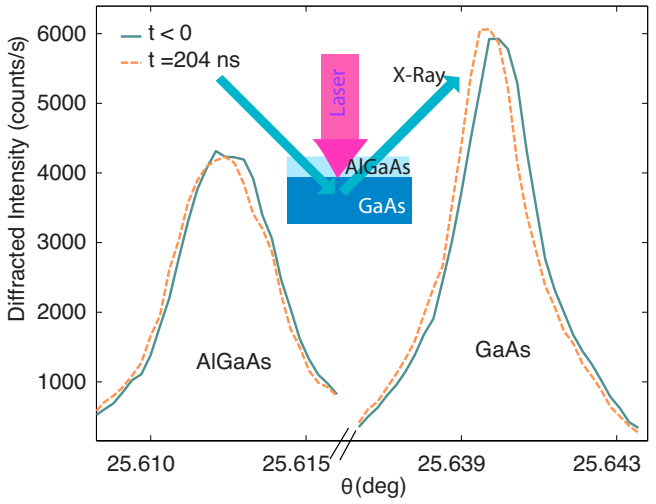


FIG. 1. (Color online) X-ray rocking curve from an $Al_{0.3}Ga_{0.7}As/GaAs$ heterostructure showing a laser-excitation-induced shifts in the angle of the 004 Bragg reflections.

photodiode is sent to a constant fraction discriminator (cfd). Three counters measure the coincidence of the output of the cfd with three sequential gates spanning a single x-ray pulse but separated by a fixed time delay $1/P0$, where $P0 \approx 272$ kHz is the repetition rate of an electron bunch in the storage ring. One gate is set near coincident with the laser which heats the sample, and the other two are set one revolution before and after the laser. Because the three counters detect x rays originating from the same electron bunch, the early x-ray pulse $(t=\Delta t-1/P0)$ can be used for normalization of the near coincident $(t=\Delta t)$ and late $(t=\Delta t+1/P0)$ x-ray signals.

The sample is a 1.5-$\mu$m-thick (001) $Al_{0.3}Ga_{0.7}As$ film grown on a $600\pm25$ $\mu$m (001) GaAs substrate by molecular-beam epitaxy, capped by a thin (50 Å) layer of GaAs. For this composition, the film is transparent to the near-infrared laser pulses but is absorbed in the GaAs substrate. In addition, the relatively low Al composition provides an excellent acoustic match with the GaAs substrate while high enough to provide confinement of the photoexcited carriers to the substrate.[15] Thus, carrier relaxation initially heats the substrate only (we estimate by at most few degrees). We follow the thermal transport by measuring the time-dependent Bragg shift due to thermal expansion of the film and substrate. Figure 1 shows typical x-ray rocking curves taken with 0.0003° step size before and 204 ns after laser excitation. Two peaks corresponding to the 004 $Al_{0.3}Ga_{0.7}As$ and GaAs reflections are resolved clearly. The angular separation between the two peaks before laser excitation is a measure of the lattice mismatch along the growth direction, $\Delta c/c \sim 9\times10^{-4}$. Using an asymmetric reflection, we measure the in-plane lattice parameter to be lattice matched to better than $10^{-5}$. Thus, the film is tetragonally strained, and we do not expect misfit dislocations to provide for a substantial increase in the boundary resistance. This is consistent with our prior conclusions that phonon propagation at the interface can be considered in the acoustic mismatch limit.[15]

Figure 2 shows the time evolution of the shift in the

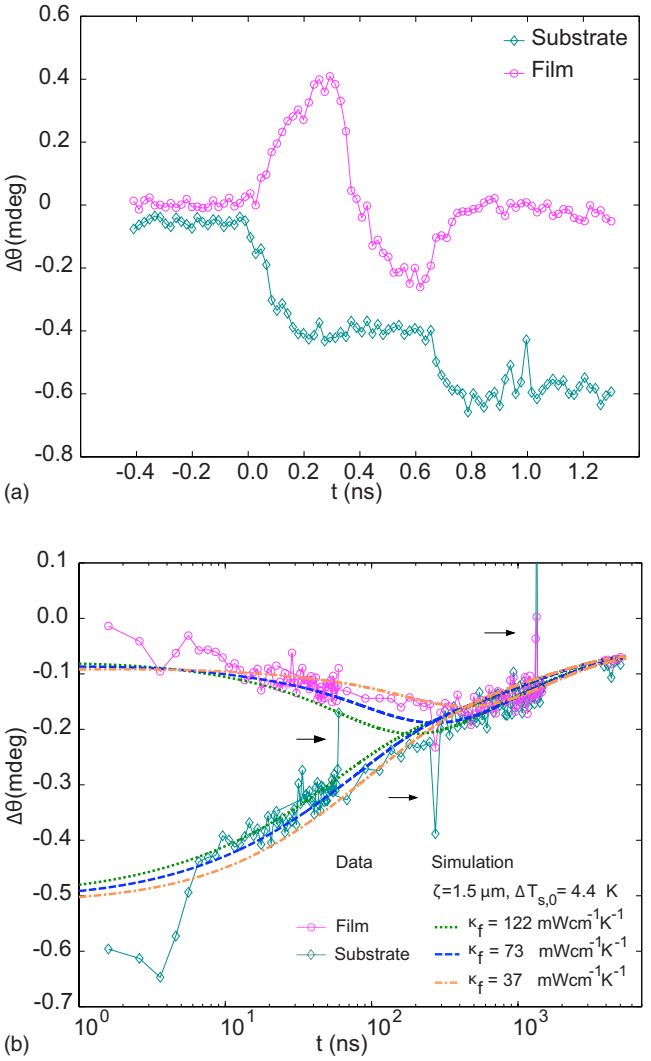


FIG. 2. (Color online) Time-resolved Bragg shift for excitation with 0.95 W average power. (a) Propagation of a coherent acoustic phonon pulse from the near instantaneous stress due to photoexcitation. (b) Data showing the heating and cooling of the film and substrate and comparison with simulations. The arrows indicate periodic coherent acoustic echoes.

Bragg angle of the film and bulk following laser excitation with an average power of 0.95 W. The negative shift in the Bragg angle, $\Delta\theta_B$, corresponds to lattice expansion and was determined by center of mass about an 18.6 mdeg window around each peak. To avoid systematic errors in positioning the diffractometer, the shift is determined relative to the early x-ray peak measured concurrently for each time delay. The systematic error in determining the center of mass due to finite sampling is much less than the minimum step size and is estimated to be negligible compared to statistical errors due to x-ray photon counting statistics and fluctuations in the laser power. At the earliest times $\lesssim 1$ ns [Fig. 2(a)], stress due to both charge carriers (deformation potential) and heat (thermal expansion) drive a coherent acoustic strain pulse that propagates into the film and the bulk.[15] Within a nanosecond, this pulse has traversed the film, reflected from the front surface and passed through the x-ray probe region of

the substrate leaving behind a region of expansion which evolves on the nanosecond to microsecond time scale [Fig. 2(b)]. During this time, there are periodic echoes as the coherent acoustic pulse travels back and forth across the ~600 $\mu$m-thick wafer (although due to the finite sampling, not all echoes are observed in the pump-probe data). The magnitude of the shift of the GaAs Bragg peak increases over a few nanoseconds as the carriers relax and heat the lattice before decreasing monotonically over several microseconds, while the magnitude of $Al_{0.3}Ga_{0.7}As$ shift first increases over a few hundred nanoseconds before decreasing and merging with the shift of the GaAs.

After the carriers have thermalized with the lattice, the shift in the Bragg peak is a measure of the average temperature profile, $\langle \Delta T \rangle$, weighted across the region probed by the x rays. In the kinematic limit,

$$\Delta \theta_B = -\alpha \langle \Delta T \rangle \tan(\theta_B), \tag{1}$$

where $\alpha$ is the linear-expansion coefficient, and we assume that the strain is approximately hydrostatic within the x-ray probe volume.[18] The ratio of the linear-expansion coefficient for the film and substrate can be determined by the ratio of the Bragg shifts (1) at long times when the film and substrate are heated approximately uniformly across the x-ray probe depth. However, because of difficulties in determining extremely small Bragg shifts, in what follows, we use literature values for the bulk thermal-expansion coefficients ($6.4 \times 10^{-6}$/K and $6.0 \times 10^{-6}$/K) for the substrate and film, respectively;[19] to the extent that the temperature rise is small our results for the thermal conductivity do not depend directly on these parameters.

We model our data assuming a rapid and differential heating of the substrate. Subsequent to this heating, we assume that the thermal transport is primarily one dimensional, as diffusion across the approximately millimeter transverse extent of the laser-excited region is slow compared to the time scale of the experiment. The initial thermal distribution is not precisely known because the details of the initial carrier distribution and its dynamics are complex, in part, because of the possibility of near-degenerate carrier concentrations due to the low effective mass and near direct-band-gap excitation. The optimum modeling of data occurs if we allow for a broader initial temperature profile than the exponential profile one would obtain for instantaneous heating across the linear absorption of the laser radiation. This could occur, for example, if the photoexcited carriers diffuse substantially before recombination. For a recombination rate of ~1 ns, the ambipolar diffusion length becomes comparable to the penetration depth (1 $\mu$m), and the initial thermal profile will be near Gaussian. Thus, to account for uncertainties in the carrier dynamics, we assume a Gaussian thermal profile and allow the peak temperature rise and root-mean-square (rms) depth to vary in our simulations.

We solve numerically the one-dimensional diffusion equation for the 1.5 $\mu$m film and a limited thickness of 20 $\mu$m of the substrate (to save computation time while being thick enough for diffusion over the time scale of experiment). The initial temperature profile is

$$\Delta T_f(z, t=0) = 0, \tag{2}$$

$$\Delta T_s(z, t=0) = \Delta T_{s,0} e^{-z^2/2\zeta^2} = \frac{Q(1-R)}{C\sqrt{2\pi}\zeta A} e^{-z^2/2\zeta^2}, \tag{3}$$

where $Q$, $R$, $C$, $\zeta$, and $A$ are the laser-pulse energy, reflectivity of the substrate, volumetric specific heat of the substrate, rms depth of the initial heat deposition, and laser spot area on the sample, respectively, and $z$ is the vertical coordinate along the sample. The interface is at $z=0$ and the subscripts $f$ and $s$ represent the film and substrate, respectively. We assume that the thermal conductivity, $\kappa$, and diffusivity are related through the specific heat (1.79 and 1.82 J/g/K for the substrate and film, respectively[19]) in kinetic theory. We model the thermal transport as heat flow across the heterostructure interface with negligible thermal boundary resistance, $\kappa_s (dT_s/dz|_{z=0}) = \kappa_f (dT_f/dz|_{z=0})$, $T_s(z=0,t) = T_f(z=0,t)$. We also assume negligible heat flow out the surface of the film and negligible temperature rise at a depth of 20 $\mu$m into the substrate, $dT_f/dz = 0$, $\Delta T_s(z=20\ \mu\text{m}, t) = 0$. The x-ray data were simulated using a dynamical theory of x-ray diffraction[20] modified to include the depth-dependent thermal strain.[13,21] In this manner, we account for the strong extinction of the x rays and the sharp gradient in the temperature profile at early times. To avoid systematic errors in the analysis, the shifts in the simulated Bragg peaks are calculated by the same center-of-mass method as the data. In order to extract the film thermal conductivity, we performed a multidimensional least-squares fit between the data and simulations with the only other free parameters being the maximum temperature rise of the substrate, $\Delta T_{s,0}$, and rms depth, $\zeta$, in Eq. (3) over a time 4.5 ns $< t <$ 5.4 $\mu$s. We fix the substrate thermal conductivity by using bulk parameter [$\kappa_s = 440$ mW/cm K (Ref. 19)] and note that the long-time behavior is primarily sensitive to this parameter.

The result of the fit is $\kappa_f = 73$ mW/cm K (dashed line in Fig. 2) with $\Delta T_{s,0} = 4.4$ K and $\zeta = 1.5$ $\mu$m. The extracted thermal conductivity is consistent in experiments made with a range of excitations from 0.25 to 2.0 W average power; however the best fit to the initial thermal profile varies both in the peak temperature rise and the depth, underscoring the complexity in the heating process. Figure 3 shows the calculated temperature profile at several times using the fit parameters for the data in Fig. 2. Note that the heat diffuses initially into both the substrate and film. After several hundred nanoseconds, the temperature profile in the film becomes nearly uniform, at which time the substrate and film cool through heat diffusion into the bulk. The evolution of the thermal profile is sensitive to both the initial heat distribution in the substrate as well as the thermal properties of the film and substrate. The effect of the initial thermal profile appears primarily at early times. In particular, as we broaden the initial thermal profile, we find that the film and near interface region of the substrate take longer to reach a common temperature because the contribution of the initial cooling through bulk diffusion becomes increasingly less important than the heating of the film.

We note that the ternary semiconductor compound $Al_xGa_{1-x}As$ shows significant bowing (i.e., nonlinear behav-

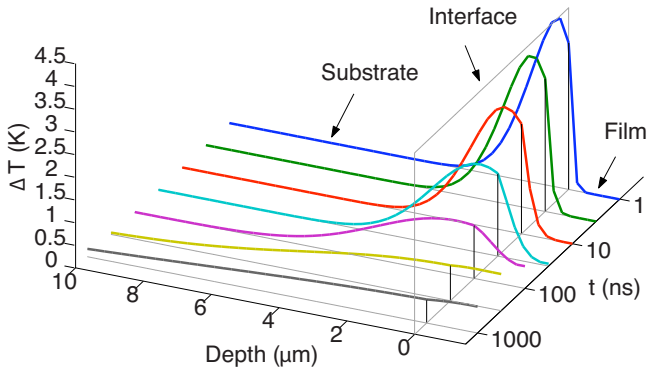


FIG. 3. (Color online) Calculated temperature distribution over the film and the first 10 $\mu$m of the substrate at different times, assuming instantaneous substrate heating across a 20 $\mu$m depth and the best fit parameters at 0.95 W.

ior with respect to the composition) in the room-temperature thermal conductivity.[22,23] Afromowitz[22] obtained the thermal conductivity for different alloys grown by liquid-phase epitaxy (LPE) by measuring a temperature gradient across a rectangular bar perpendicular to the growth direction. The results were in good agreement with the theoretical model of Abeles[24] that accounted for the increased thermal resistivity of a disordered alloy (over the average value of the composition) due to strain and mass point-defect scattering of phonons. In this case the strain scattering was found to be negligible because of the excellent lattice match between AlAs and GaAs. More recently Pichardo *et al.*[23] extracted the thermal conductivity using a photoacoustic technique for LPE samples of differing thickness on GaAs (001) substrates and fitted their data to find the bowing parameter given by Adachi.[19] In particular, Adachi[19] showed that Abele's model can be incorporated as a single nonlinear term in the thermal resistivity of a ternary alloy, $\kappa^{-1}=x\kappa_A^{-1}+(1-x)\kappa_B^{-1}+x(1-x)C_{A-B}$, due to random disorder in the Al($A$) and Ga($B$) sites. The data from Pichardo *et al.*[23] and Afromowitz[22] are in reasonable agreement, although Pichardo *et al.*[23] measured slightly higher (lower) thermal resistivity (conductivity) for $x \leq 0.5$ and the opposite for $x > 0.5$. Using these combined data, Adachi[25] extracted a value of $C_{A-B}=0.032$ cm K/mW (0.030 cm K/mW for the Afromowitz data alone[19]). If we compare our results with the extrapolated thermal conductivity for $x=0.3$ (122 mW/cm K), we find that our value is about 40% lower than expected.

Because of uncertainties in the initial thermal deposition, it is difficult to assign an appropriate error bar directly from the fit. In order to explore the sensitivity of our technique, we compare the results of the simulation for three different values of the thermal conductivity using the same initial temperature profile. Note that for the higher conductivity [$\kappa_f$ =122 mW/cm K, dotted line Fig. 2(b)], the model deviates from the data, most notably in overestimating the Bragg shift during heating of the film and underestimates the time at which the film begins to cool. For a smaller thermal conductivity ($\kappa_f$=37 mW/cm K, 30% of the expected value), a somewhat different deviation is seen: the cooling of the substrate is overestimated and the time in which the film begins to cool is delayed.

In our simulations, we have assumed an infinite thermal boundary conductance due to the excellent acoustic match at the $Al_{0.3}Ga_{0.7}As/GaAs$ interface. In principle, our technique can measure the thermal boundary conductance directly, as we measure the (average) temperature on either side of the interface, albeit the effect would be much easier to quantify for an interface of highly dissimilar materials. A finite thermal boundary conductance will affect primarily the thermal transport at early times when there is substantial heat flow. However, this is also the time during which there are substantial spatial variations in the thermal profile, so the temperature drop immediately across the interface must still be modeled. To have a noticeable effect on our results, we find that the thermal boundary conductance needs to be $\lesssim 10^4$ W/cm$^2$ K at least 2 orders of magnitude less than we estimate in the acoustic mismatch limit.[3] Based on the quality of the interface and our previous studies on the strain propagation, we believe that this possibility can be excluded.

Thus, we conclude that while the difference between our thermal-conductivity measurement and the extrapolation from the LPE data is relatively small, it is significant. The lower than bulk thermal conductivity of a heterostructure can be attributed to several mechanisms including scattering from defects and dislocations, lattice strain, and finite-size effects. As discussed below, we do not expect that any of these mechanisms to substantially affect the thermal conductivity of our relatively thick $Al_{0.3}Ga_{0.7}As$ film. Because alloy scattering dominates the thermal resistivity, we do not expect differences in defect density to play an important role, unless there are substantial differences in alloy ordering. While it is known that AlGaAs grown by metal-organic vapor-phase epitaxy have been known to form ordered alloys under certain conditions,[26] both MBE and LPE grown samples are likely to be a random alloy.[27,28]

Abramson *et al.*[1] proposed the possibility of strained interface might be responsible for the reduced thermal conductivity of heterostructure due to changes in the interatomic forces and as well as phonon-phonon interactions. On the other hand, in the model developed by Afromowitz[22] scattering contributed from strain is much smaller compared to point-defect scattering due to large atomic mass difference of Al and Ga in AlGaAs alloy. While we find that the film is fully tetragonally strained, it is only $\sim 4.1\times 10^{-4}$, such that we do not anticipate that this will contribute substantially to the thermal conductivity.

Recently, Highland *et al.*[4] utilized a combination of thermoreflectance and the atomic resolution of TRXD to study the contribution of ballistic phonons to heat propagation in 120–250-nm-thick InGaAs buried layers. They found that ballistic phonons account for nearly 20% of the heat flow across the buried layer within nanoseconds after femtosecond laser heating of a metallic transducer. In our case, the density of states of ballistic phonons is likely much smaller due to the thicker film and relatively large aluminum content of the alloy.

In our simulations, we assume a kinetic theory for the transport, effectively assigning an average mean free path for the phonons. In addition, by assigning an average temperature from the thermal expansion, we assume that the anharmonicity of the modes that contribute most to the heat flow is

also responsible primarily for the thermal expansion. Further, while the heat flow is one dimensional on the time scale of these experiments, the strain is uniaxial over the x-ray probe region only at very short times.[18] Although we do not believe that this would substantially affect our results, it would be valuable to measure the development of the in-plane component of the strain to more accurately determine the temperature profile over the full temporal range of the experiment.[29]

In conclusion, we use a combination of ultrafast laser excitation and time-resolved x-ray diffraction to study the thermal transport following carrier recombination in an (001) $Al_{0.3}Ga_{0.7}As/GaAs$ heterostructure grown by MBE. Using an initial Gaussian heat profile to account for the complexity of the photoexcited carrier dynamics in the substrate, we model the bidirectional heat transport across the interface and extract the film thermal conductivity.

This work was conducted at the sector 7 insertion device beamline at the APS and was supported in part by the U.S. DOE Grant No. DE-FG02-00ER1503 and from the NSF FOCUS physics frontier center. We thank Eric Dufresne for experimental assistance. M.R. and R.S.G. acknowledge partial support of the NSF Focused Research Group through Grant No. 0606406. Use of the Advanced Photon Source was supported by the Office of Science, Office of Basic Energy Sciences, U.S. Department of Energy under Contract No. DE-AC02-06CH11357.

*Present address: Department of Physics, DePaul University, 211 Byrne Hall, 2219 N. Kenmore, Chicago, Illinois 60614, USA.

[1] A. R. Abramson, C.-L. Tien, and A. Majumdar, J. Heat Transfer **124**, 963 (2002).
[2] D. G. Cahill and F. Watanabe, Phys. Rev. B **70**, 235322 (2004).
[3] E. T. Swartz and R. O. Pohl, Rev. Mod. Phys. **61**, 605 (1989).
[4] M. Highland, B. C. Gundrum, Y. K. Koh, R. S. Averback, D. G. Cahill, V. C. Elarde, J. J. Coleman, D. A. Walko, and E. C. Landahl, Phys. Rev. B **76**, 075337 (2007).
[5] S.-i. Tamura, Y. Tanaka, and H. J. Maris, Phys. Rev. B **60**, 2627 (1999).
[6] W. S. Capinski, H. J. Maris, T. Ruf, M. Cardona, K. Ploog, and D. S. Katzer, Phys. Rev. B **59**, 8105 (1999).
[7] D. G. Cahill, W. K. Ford, K. E. Goodson, G. D. Mahan, A. Majumdar, H. J. Maris, R. Merlin, and S. R. Phillpot, J. Appl. Phys. **93**, 793 (2003).
[8] C. Thomsen, H. T. Grahn, H. J. Maris, and J. Tauc, Phys. Rev. B **34**, 4129 (1986).
[9] R. J. Stoner and H. J. Maris, Phys. Rev. B **48**, 16373 (1993).
[10] B. C. Daly, H. J. Maris, W. K. Ford, G. A. Antonelli, L. Wong, and E. Andideh, J. Appl. Phys. **92**, 6005 (2002).
[11] R. M. Costescu, M. A. Wall, and D. G. Cahill, Phys. Rev. B **67**, 054302 (2003).
[12] T. Yao, Appl. Phys. Lett. **51**, 1798 (1987).
[13] D. A. Reis and A. M. Lindenberg, in *Light Scattering in Solids IX, Topics in Applied Physics*, edited by M. Cardona and R. Merlin (Springer, New York, 2007), Vol. 108, pp. 371–422.
[14] D. M. Fritz, D. A. Reis *et al.*, Science **315**, 633 (2007).
[15] S. H. Lee, A. L. Cavalieri, D. M. Fritz, M. C. Swan, R. S. Hegde, M. Reason, R. S. Goldman, and D. A. Reis, Phys. Rev. Lett. **95**, 246104 (2005).
[16] D. A. Reis, M. F. DeCamp *et al.*, Phys. Rev. Lett. **86**, 3072 (2001).
[17] M. F. DeCamp, D. A. Reis, D. M. Fritz, P. H. Bucksbaum, E. M. Dufresne, and R. Clarke, J. Synchrotron Radiat. **12**, 177 (2005).
[18] Locally the strain is hydrostatic on times longer than sound propagation across the x-ray spot ($\gtrsim$50–100 ns). In our experiments there is a crossover between nonhydrostatic and hydrostatic strains that can lead to an overestimation of the temperature at early times. Thus our analysis gives an upper bound for the thermal conductivity.
[19] S. Adachi, J. Appl. Phys. **58**, R1 (1985).
[20] B. W. Batterman and H. Cole, Rev. Mod. Phys. **36**, 681 (1964).
[21] C. R. Wie, T. A. Tombrello, and T. Vreeland, Jr., J. Appl. Phys. **59**, 3743 (1986).
[22] M. A. Afromowitz, J. Appl. Phys. **44**, 1292 (1973).
[23] J. Pichardo, J. Alvarado-Gil, A. Cruz, J. Mendoza, and G. Torres, J. Appl. Phys. **87**, 7740 (2000).
[24] B. Abeles, Phys. Rev. **131**, 1906 (1963).
[25] S. Adachi, J. Appl. Phys. **102**, 063502 (2007).
[26] T. S. Kuan, T. F. Kuech, W. I. Wang, and E. L. Wilkie, Phys. Rev. Lett. **54**, 201 (1985).
[27] Y. Kashihara, N. Kashiwagura, M. Sakata, J. Harada, and T. Arii, Jpn. J. Appl. Phys., Part 2 **23**, L901 (1984).
[28] C. Bocchi, P. Franzosi, and C. Ghezzi, J. Appl. Phys. **57**, 4533 (1985).
[29] E. M. Dufresne, B. Adams, E. C. Landahl, A. M. Khounsary, D. Reis, D. M. Fritz, and S-H. Lee, in *Synchrotron Radiation Instrumentation: Ninth International Conference on Synchrotron Radiation Instrumentation*, edited by J-Y. Choi and S. Rah, AIP Conf. Proc. No. 879 (AIP, Melville, NY, 2007), p. 1210.